Overcoming the challenges of accessing topological hallmarks in Sb(112)

To cite this article: A C Åsland *et al* 2025 *Electron. Struct.* **7** 035002

IOP Publishing Electron. Struct. 7 (2025) 035002 https://doi.org/10.1088/2516-1075/adf384

Electronic Structure

OPEN ACCESS

RECEIVED
16 March 2025

REVISED
20 July 2025

ACCEPTED FOR PUBLICATION
23 July 2025

PUBLISHED
19 August 2025

PAPER

Overcoming the challenges of accessing topological hallmarks in Sb(112)

A C Åsland[1,*], J Bakkelund[1], S P Cooil[2], H I Røst[3], J Hu[1], E Vescovo[4], A Rajapitamahuni[4], F Mazzola[5,6] and J W Wells[1,2,*]

[1] Department of Physics, Norwegian University of Science and Technology (NTNU), NO-7491 Trondheim, Norway
[2] Centre for Materials Science and Nanotechnology, University of Oslo, NO-0318 Oslo, Norway
[3] Department of Physics and Technology, University of Bergen, NO-5007 Bergen, Norway
[4] National Synchrotron Light Source II, Brookhaven National Laboratory, Upton, NY, United States of America
[5] Istituto Officina dei Materiali (IOM)-CNR, Area Science Park-Basovizza, S.S. 14 Km 163.5, 34149 Trieste, Italy
[6] Department of Molecular Sciences and Nanosystems, Ca' Foscari University of Venice, 30172 Venice, Italy
[*] Authors to whom any correspondence should be addressed.

E-mail: annacecilieasland@gmail.com and j.w.wells@fys.uio.no

Keywords: antimony, vicinal surfaces, topology, spin polarisation, ARPES

Supplementary material for this article is available online

Abstract

Sb is topologically non-trivial and semi-metallic, but differs from many topological semi-metals because of its continuous band gap. By measuring its (112) surface using angle- and spin-resolved photoemission spectroscopy, Sb(112) was shown to have 1D spin-polarised surface states resembling those on vicinal Bi surfaces and many topological insulators and topological semi-metals. The shape and spin-polarisation of the measured features and the calculated bands agreed. However, the measured features had a slightly steeper energy dispersion and different Fermi-momenta than the calculated bands. Both theoretical and experimental methods were necessary when determining the topology of Sb(112). The presence of projected bulk states near the Fermi-level and varying surface localisation of the electronic states meant it was challenging to deduce the topology of Sb(112) from the number of bands crossing the Fermi-level or a continuous contour in the bulk band gap. Ultimately, the calculations and measurements suggest that there are topological surface states on the Sb(112) surface.

1. Introduction

The study of topological insulators (TIs) and topological semi-metals (TSMs) has been one of the most active and successful areas of condensed matter research in the past few decades [1–5]. Currently, such materials attract interest for their use in a range of applications, including spintronics, thermoelectrics, terahertz sensing, advanced electronics and optoelectronics [4, 6–14]. In short, TIs are insulators in the bulk, but their non-trivial topology means that they have robust spin-polarised metallic surface or edge states in which electrons are protected from backscattering [3, 15–17]. TSMs have bulk bands crossing the Fermi-level (E_F), however, non-trivial topology caused by band inversions can result in interesting features on their Fermi-surfaces (FSs) and intriguing physical phenomena [2, 5]. Elemental Sb is topologically non-trivial and semi-metallic, and can therefore be considered a TSM [18–21]. In most TSMs, the transition into a topologically non-trivial state happens because the conduction band (CB) touches the valence band (VB) [5]. However, Sb has a continuous band gap and is semi-metallic because the CB and VB cross the E_F at different momenta (**k**) in the Brillouin zone (BZ) [18, 21]. Changing the thickness or spin-orbit-coupling of Sb has been predicted to cause transitions between different topological phases [21–24]. Such transitions have been verified experimentally by the presence of topological states on thin films of Sb and from alloying Sb with Bi to create $Bi_{1-x}Sb_x$, which was the first experimentally confirmed 3D TI [19, 20, 22, 25–31]. Furthermore, some surfaces of Sb crystals have been shown to possess spin-polarised surface states, which is one of the characteristics of topologically non-trivial materials [32–35]. Although these surface states

generally follow the predictions from topology, Bianchi *et al* suggested that conventional topological arguments become invalid along crystal directions where the surface is metallic [21, 34]. This means that despite the many indications of topological surface states on Sb, it is unclear how its topological nature can be determined from such arguments.

In the work herein, we have investigated the surface states on Sb(112) using spin- and angle-resolved photoemission spectroscopy (SARPES) and tight-binding (TB) calculations. The surface states were found to be nearly 1D and spin-polarised, thus reminiscent of those on many TIs, TSMs, higher order TIs (HOTIs) and also on the vicinal surfaces of its topologically trivial sister compound Bi [36–49]. It was challenging to determine the topology of the surface states on Sb(112) from the measurements or calculations alone, due to the presence of bulk states near the E_F and since the surface character of the bands in the band structure can vary along the band. A good understanding of both the calculations and the measurements is therefore required when studying the topology of semi-metals like Sb.

2. Methods

The Sb(112) crystal was cleaned by repeated cycles of Ar^+ ion sputtering at 200−600 eV and annealing to $T \approx 250\,^{\circ}\mathrm{C}$ for 5−20 min. X-ray photoelectron spectroscopy (XPS) and low energy electron diffraction (LEED) confirmed that the surface was clean and crystalline [50]. Its band structure and spin-polarisation were measured using SARPES and calculated using a TB model as detailed in the Supplementary Material (SM) [50].

2.1. Momentum microscopy measurements

The band structure and spin-polarisation in figures 2(g) and 3(c), (d), (g) and (h) were measured using a NanoESCA III aberration corrected EF-PEEM with an Au-coated Ir spin-filter as detailed in [46, 51, 52]. With photoexcitation energy of $h\nu = 21.2$ eV, pass energy $E_P = 25$ eV and a 1.0 mm entrance slit to the energy filter, the energy and momentum resolutions of the instrument were approximately 100 meV and 0.02 $\mathrm{Å}^{-1}$, respectively. Band structure measurements were performed at a temperature of $T \approx 120$ K, and the spin-filtered measurements at room temperature ($T \approx 300$ K). When calculating the spin-polarisation, a Sherman function of $S = 0.6$ was assumed based on calibration measurements [52]. Further details about the spin-filtered measurements and how the spin-polarisation was calculated have been included in the SM [50].

2.2. High-resolution measurements

Higher-energy-resolution band structure measurements were performed at Beamline 21-ID (ESM) at NSLS II of Brookhaven National Labs , U.S., and at the APE-LE endstation of Elettra Synchrotron Trieste, Italy. Both facilities used a VG SCIENTA DA30 analyser and the samples were kept at a temperature of $T \approx 20$ K during the measurements.

The spin measurements in figures 3(e) and (f) were performed at Elettra using two VLEED spin-detectors and assuming a Sherman function of $S = 0.3$ from calibration measurements. Details about the experimental set-up and how the spin-polarisation was calculated can be found in [46] and [53], and in the SM [50].

3. Results & discussion

The topological nature of a 3D crystal can be defined in terms of $\mathbb{Z}_2$-parameters calculated from the parity eigenvalues $\delta(\Lambda)$ of the occupied energy bands at high symmetry points Λ (a.k.a. time-reversal invariant momenta or TRIMs) in the bulk BZ [19, 20]. Similarly, the topological nature of a given surface can be determined from the surface parity eigenvalues $\pi(\overline{\Lambda})$ at surface TRIMs $\overline{\Lambda}$, calculated from the bulk parity eigenvalues projecting onto the surface, as visualised in figure 1(a) [20, 54]. Topologically trivial and non-trivial materials can be distinguished by whether or not their electronic bands can be continuously deformed until they are pushed into the CB or VB [16]. This is related to the way spin-split bands are connected at spin-degenerate TRIMs, and can be determined by counting the number of bands crossing the E_F for insulators which have the E_F entirely in the bulk band gap [16]. If two surface TRIMs have different parity, an odd number of E_F crossings—and therefore, topological surface states, are expected between the two [54]. Contrarily, pairs of surface TRIMs with the same parity should yield an even number of E_F crossings and topologically trivial surface states [54]. A similar approach has previously been used to suggest the topology of semi-metals [34]. However, since the CB or VB can extend below or above the E_F, respectively, it is possible to have deformable (trivial) bands which only cross E_F once, or non-deformable (topological) bands which do not cross E_F at all. A schematic example has been given in figure 1(b) where the leftmost red and blue bands are topologically non-trivial, and the rightmost red and blue bands are trivial. Despite this, in total there is an even number of E_F crossings (two red band crossings) between the two

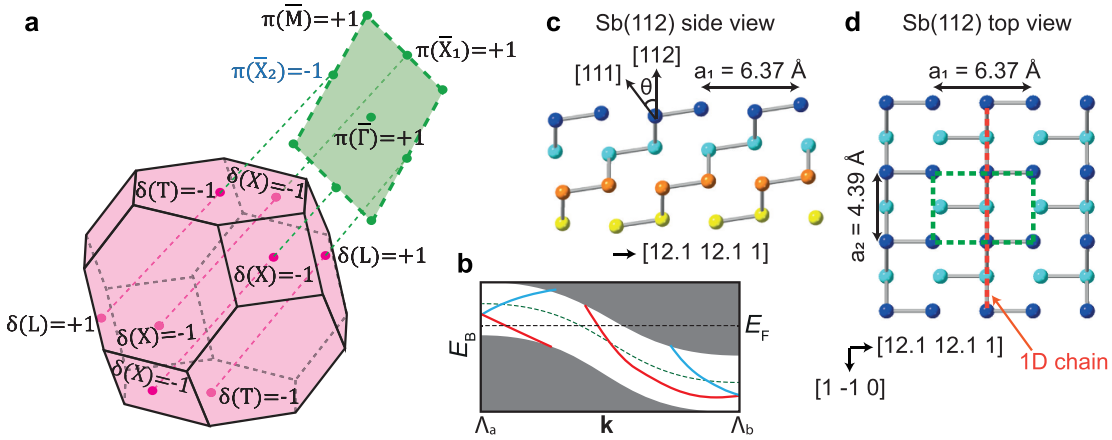

Figure 1. (a) Bulk Brillouin Zone (BZ) of Sb (pink) and the projected BZ of the Sb(112) surface (green). The parity eigenvalues at bulk ($\delta(\Lambda)$) and surface ($\pi(\overline{\Lambda})$) time-reversal invariant momenta (TRIMs, Λ, $\overline{\Lambda}$) have been indicated based on [19, 20, 54]. (b) Sketch of a band structure (E_B vs. **k** plot) between TRIMs Λ_a and Λ_b for a semi-metallic material with non-trivial topology. The conduction band dips below the E_F indicated by the black dashed line. The green dashed line shows an example of a continuous contour in the bulk band gap. (c), (d) Atomic structure of Sb(112) seen from the side (c) and the top (d).

TRIMs, which would naïvely lead to the incorrect conclusion of topologically trivial behaviour. For semi-metals with a continuous band gap, an alternative approach could be to count the number of bands that cross a continuous contour which varies in energy but remains in the gap. See, for example, the contour drawn as a dark green dashed line in figure 1(b) which has three bands crossing it, and correctly suggests that the topology is non-trivial. In this paper, the number of both E_F crossings and 'contour crossings' has been considered for Sb(112) and used to investigate its topology.

The atomic structure of Sb(112) has been shown in figures 1(c) and (d). Edges of Sb(111) surface planes are exposed on the surface and form 1D chains of atoms along the [1–10] direction. LEED measurements confirmed the crystal structure (see the SM for further details [50]). Its projected BZ has four surface TRIMs, $\overline{\Gamma}$, $\overline{X}_1$, $\overline{X}_2$ and $\overline{M}$, with surface parities of $\pi(\overline{\Gamma}) = +1$, $\pi(\overline{X}_1) = +1$, $\pi(\overline{X}_2) = -1$ and $\pi(\overline{M}) = +1$, respectively, as shown in figure 1(a). Since the surface parity of $\overline{X}_2$ is different from the remaining three surface TRIMs, an odd number of E_F (or contour) crossings and topological surface states were expected for paths between $\overline{X}_2$ and any other surface TRIM. Between $\overline{\Gamma}$, $\overline{X}_1$ and $\overline{M}$, an even number of E_F (contour) crossings was expected. Sb has bulk inversion symmetry, hence, its bulk states are spin-degenerate [18]. Since spin-degenerate bands contribute with an even number of E_F (contour) crossings, only surface states, for which the inversion symmetry is broken due to the surface, have been considered for the topological arguments.

3.1. Calculated Band Structure

The band structure of Sb(112) was calculated using a TB model (described in detail in the SM [50]) and has been presented in figures 2(a)–(f). In figures 2(a), (b) and (f) the electronic states have been shaded according to their surface localisation (darker states are more surface localised). The grey continuum in figures 2(c)–(e) consists of states with an overall weak surface localisation, thus, they have the characteristics of bulk states [55, 56]. The coloured bands labelled 1–7 in figures 2(c)–(e) are fully or partly in the bulk band gap and are generally more surface localised than the grey states, i.e. they are reminiscent of surface bands [55, 56]. However, some of the bands, e.g. band 1 (light blue) in figure 2(c) and bands 5 (pink), 6 (purple) and 7 (orange) in figure 2(d), are surface localised in the bulk band gap, but are less surface localised where they overlap with the continuum of projected bulk states near $\overline{X}_2$. Hence, the bands have parts with bulk character even if they are predominantly surface-like. In other words, there are some values of binding energy (E_B) and **k** where the electrons in 'surface bands' have a lower probability of existing at the surface. Furthermore, some of the bands in the bulk continuum have more surface localised states even if the majority of the states in the band are weakly surface localised. This gives rise to dark features like the one centred at $\overline{X}_2$ in figure 2(b) (marked with dark blue solid arrows), and indicates that electrons in some 'bulk' states exist at the surface. Since the surface localisation of the bands can vary, it is not immediately clear which bands should be counted as E_F crossings. Furthermore, it can be unclear where the bulk band gap is and where a continuous contour should be drawn.

There are no bulk bands at the calculated E_F (E_F^c, black dashed line) in figures 2(a) and (c), and only bands 3 and 4 cross E_F^c near $\overline{\Gamma}$. Thus, there is unambiguously an even number of E_F^c, and equivalently contour, crossings between $\overline{\Gamma}$ and $\overline{X}_1$ as expected from the surface parity eigenvalues.

Between $\overline{X}_2$ and $\overline{M}$ in figures 2(b) and (d), the bulk continuum crosses E_F^c near both $\overline{X}_2$ and $\overline{M}$, hence, conventional topological arguments might not apply [21, 34]. If the topology of the surface could be determined by counting the number of *surface* band E_F crossings, one could argue that only band 7 exists in the bulk band gap at the E_F^c (see figure 2(e)) and is, therefore, the only surface state. In this case, there would be an odd number of E_F^c crossings between $\overline{X}_2$ and $\overline{M}$, in agreement with the expectations from parity considerations. However, from figures 2(b) and (f) it can be seen that there are surface localised states in the bulk continuum (from the feature marked by dark blue solid arrows) crossing the E_F^c. If these are counted as surface states it is possible to count an even number of E_F^c crossings. If the overall character of a given band is considered, bands 5, 6 and 7 are all surface bands crossing the E_F^c twice between $\overline{X}_2$ and $\overline{M}$ in figures 2(d) and (e). This would give an even number of E_F^c crossings and presumably topologically trivial surface states. Contrarily: if the electron occupancy of the bands changed such that E_F^c were to reside where $E_B \gtrsim 0.1$ eV in figures 2(d) and (e), bands 5–7 would all contribute with one E_F^c crossing each, resulting in an odd number of crossings. Similarly, between $\overline{\Gamma} - \overline{X}_1$ in figure 2(c), either 3 or 4 crossings could be achieved if $E_F^c = E_B \gtrsim 0.2$ eV. In any case, the mixed nature of the states and any uncertainty in E_F make it challenging to unambiguously determine the number of E_F crossings along the important high symmetry directions.

One cannot ascertain the topology of the calculated surface states on Sb(112) from the number of E_F^c crossings alone because it is unclear whether one should consider (*i.*) only surface localised bands existing in the bulk band gap, (*ii.*) bands within the bulk continuum that are more surface localised near E_F^c, or (*iii.*) surface-like bands that partly exist in the bulk band gap, but overlap with bulk states and are only weakly surface localised at E_F^c. The number of E_F^c crossings also appears to depend on the electron occupancy of the calculated bands, (i.e. where the E_F^c is placed along the binding energy axis in the E_B vs. $\mathbf{k}_x$ plots): This is surprising because the topology of a material with a continuous bulk band gap should not change unless the band gap is closed [21]. For TIs in which the E_F is within the bulk band gap, the number of E_F crossings is also independent of small shifts in the E_F caused by a change in electron occupancy [16]. The apparent dependence of the number of crossings on electron occupancy is a consequence of the E_F not being entirely in the bulk band gap, and not an argument that the topology actually changes.

A better approach is to look at the number of contour crossings of a contour which lies within the bulk band gap. The bulk bands in the VB and CB appear to merge with each other near $\overline{X}_2$, making it difficult to determine where the bulk band gap is and therefore where the contour should be drawn. Sb has a continuous bulk band gap, and this apparent merging of the VB and CB is a consequence of projecting bulk bands with differing $\mathbf{k}_z$ onto the (112) surface [56].

In figures 2(b) and (d)–(f) the CB is below the E_F^c at $\overline{X}_2$, while the VB is above the E_F^c near $\mathbf{k}_x \pm 0.1$ Å^{-1}. A continuous contour is chosen to be approximately half way between the VB and CB, and between band 6 (purple) and band 7 (orange) where the VB and CB appear to merge, as indicated by the blue dotted line in figures 2(b) and (d)–(f). Bands 5 and 6 follow the edge of the VB, have weak surface localisation in the region shown in figures 2(e) and (f), and do not seem to cross the contour in the bulk band gap. Band 7 also follows the shape of the VB for $\mathbf{k}_x \gtrsim 0.1$ Å^{-1}, but it crosses the contour and merges with the CB around $\mathbf{k}_x \approx 0.1$ Å^{-1}. The merging point has been indicated by the dark blue circle in figures 2(e) and (f). Based on the colouring of the bands, band 7 appears to follow the edge of the CB between $\mathbf{k}_x \lesssim 0.1$ Å^{-1} and $\mathbf{k}_x = 0$ Å^{-1} ($\overline{X}_2$). However, when looking at the surface localisation in figure 2(f), there are more surface localised (darker) states following on from the states in band 7. The surface localisation of these states is similar to that of band 7 before it merges with the CB, and can potentially suggest that band 7 continues along the higher surface localisation states into the CB. In any case, band 7 appears to only cross the contour once. Band 7 cannot be pushed into the VB or CB without changing its connectivity, hence, it acts as a topologically non-trivial surface state between $\overline{X}_2$ and $\overline{M}$.

3.2. Measured band structure

The band structure as measured using ARPES has been shown in figures 2(g)–(l). In the measurements, only bands below the measured E_F (E_F^m) can be observed, and the entire bulk band gap may not be visible. Thus, it may not be possible to verify a continuous contour in the gap, and one has to rely on the number of E_F^m crossings when investigating the topology. In the following, only *surface* bands existing in the bulk band gap at the E_F^m has been considered as crossings. A comparison with the calculations follows at the end of the section.

The measurements were performed with different photoexcitation energies $h\nu$ to separate bands of surface and bulk character [57]. A more complete overview has been included in the SM [50]. Bulk bands disperse with out-of-plane momentum $\mathbf{k}_z$—and thus, with $h\nu$, while surface bands are $\mathbf{k}_z$-independent and

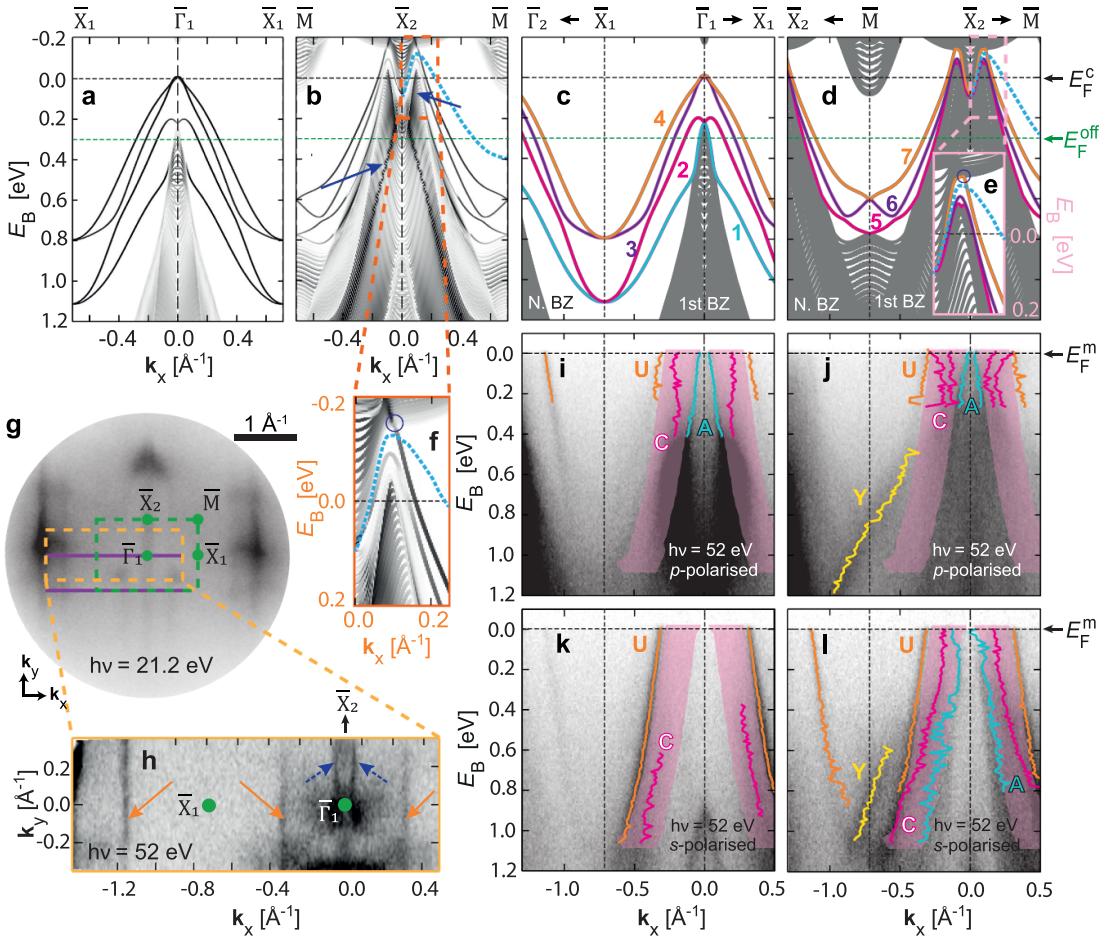

Figure 2. TB calculated (a)–(f) and measured (g)–(l) band structure of Sb(112). (a)–(d) E_B vs. $\mathbf{k}_x$ plots along $\overline{\Gamma}$ and $\overline{X}_1$ (a) and (c), and $\overline{X}_2$ and $\overline{M}$ (b) and (d). The green dashed line at $E_B = 0.3$ eV, labelled E_F^{off}, suggests a position of the calculated E_F (E_F^c) matching better with the measured E_F (E_F^m) (see details in the text). The blue dotted line in (b), (d), (e) and (f) indicates a continuous contour in the bulk band gap. (a) and (b) The shade of grey indicates the degree of surface localisation of the states (darker means more surface localised). (c) and (d) The light blue, pink, purple and orange bands labelled 1–7 are surface-like and exist in the bulk band gap. Bands with weaker surface localisation (grey) are considered bulk-like (see the SM [50] and main text). (e) and (f) Zoom of the dashed orange (b) and pink (d) rectangles. (g)–(l) ARPES measurements at $h\nu = 21.2$ eV (g), $h\nu = 52$ eV (h) and $h\nu = 50$ eV (i)–(l), and with *p*-polarised (h)–(j), *s*-polarised (k) and (l) light. (g) and (h) Constant energy surfaces (ESs) at $E_B = 0$ eV . The dashed green rectangle in (g) shows the 1st BZ with surface TRIMs. The higher-resolution FS in (f) corresponds to the orange dashed rectangle in (g). The purple lines in (g) show the directions in **k**-space where E_B vs. $\mathbf{k}_x$ plots in (i)-(l) have been measured. Coloured lines labelled A (light blue), C (pink), U (orange) and Y (yellow) in (i)-(l) show the E_B vs. $\mathbf{k}_x$ dispersion of the measured features. The pink region indicates where bands assigned to C are found. Features U and A form 1D surface states indicated in (h) by solid orange and dashed blue arrows, respectively. Near E_F^m and E_F^{off}, feature A is thought to correspond to band 1 and the feature indicated by dark blue solid arrows in (b). Feature C is assigned to bands 2, 3, 5 and 6, and feature U to bands 4 and 7. At larger E_B, feature A is thought to correspond to band 1 or bulk bands, feature C to bands 1 and 2, feature U to band 2, and feature Y to bands 6 and 7 (See the main text and SM for details [50]).

non-dispersive with $h\nu$ [55, 57–59]. Only the seemingly $\mathbf{k}_z$-dispersionless energy states within the bulk bandgap has been considered surface states that can contribute as E_F crossings.

The FS of Sb(112) in figures 2(g) and (h) shows that there are at least two pairs of nearly 1D states (solid orange and dashed dark blue arrows) on either side of the $\overline{\Gamma} - \overline{X}_2$ symmetry line. These are reminiscent of the 1D states on vicinal Bi surfaces [38, 41, 46], many TIs [36, 37] and nodal line TSMs [39, 42, 45], and also of hinge states on 3D HOTIs [43, 44, 47–49]. The origin of the 1D electronic states is thought to be the atomic chains on the Sb(112) surface, formed by edges of Sb(111) surface planes (see figures 1(c) and (d)). The one-dimensionality of these states is speculated to give rise to anisotropic transport properties [46]. The similarity to hinge states on HOTIs could suggest that bulk Sb, like bulk Bi, would be a HOTI if it was insulating [43, 44]. Still, Sb is different to Bi because it is topologically non-trivial already in the first order (based on the $\mathbb{Z}_2$-parameters proposed by Fu and Kane) [19, 20]. Sb is therefore primarily classified as a $\mathbb{Z}_2$ TSM and is expected to have 2D surface states in addition to these hinge states.

There are four distinguishable features in the E_B vs. $\mathbf{k}_x$ plots of the Sb(112) band structure shown in figures 2(i)–(l). The features are labelled A (light blue), C (pink), U (orange) and Y (yellow). The E_B vs. $\mathbf{k}_x$ dispersion of the features was determined by fitting Lorentzian functions to momentum distribution curves

at each E_B to deduce the $\mathbf{k}_x$ of the band intensity maxima. Details of how the dispersion of the features was determined, about measurements at other photoexcitation energies and a discussion of the surface or bulk character of the features, have been included in the SM [50].

Feature U is the sharpest and most prominent of the measured features, and gives rise to the outermost 1D states (solid orange arrows) in figure 2(h). Since U was found to not disperse with $h\nu$, it is recognised as a surface state. Additionally, U remains in the bulk band gap, and can therefore be counted as a E_F crossing both between $\overline{\Gamma} - \overline{X}_1$ and $\overline{X}_2 - \overline{M}$.

The second pair of 1D states (dashed dark blue arrows) in figure 2(h) corresponds to feature A in figures 2(i)–(l). Feature A appears to be surface-like for $E_B \lesssim 0.4\,\text{eV}$ between $\overline{\Gamma} - \overline{X}_1$ [50]. At larger E_B and between $\overline{X}_2 - \overline{M}$, A is in a region with bulk bands (see figures 2(j) and (l), or the SM [50]), suggesting A has bulk character.

When comparing the measured and calculated bands in figure 2, their shapes appear similar. Still, their electron occupation (or E_F) is slightly different, and the measured bands have a steeper $E_B(\mathbf{k}_x)$ dispersion than the calculated bands. Such differences can occur for several reasons, e.g. if there are slight differences between the surface structure of the model compared to the actual sample [46]. LEED measurements indicate the surface structure of the Sb(112) crystal used is generally similar to that of a truncated bulk surface (see details in the SM [50]). However, further investigations would be required to verify this. It should also be noted that assumptions in the TB calculations can result in uncertainties in the energy of the bands, even if the model describes the band structure well qualitatively [60]. Band structure calculations of vicinal surfaces can be particularly challenging to perform, and thus, discrepancies are not surprising [46].

The calculated Fermi-momenta ($\mathbf{k}_F^c$), would be in better agreement with the measured Fermi-momenta ($\mathbf{k}_F^m$) if the calculated electron occupancy had been such that $E_F^c = E_B \approx 0.3\,\text{eV}$ (green dashed lines) in figures 2(a)–(d) [50]. This energy has been labelled E_F^{off} in figures 2(a)–(d). A detailed explanation of how E_F^{off} was determined has been included in the SM [50]. Even if the varying surface localisation means that the number of E_F crossings appears to change with electron occupancy in the calculations, it is not expected to change the number of contour crossings or the topology of the material. E_F^{off} is primarily used as a tool to relate the measured and calculated bands.

Feature U in the measurements corresponds to bands 4 and 7 in the TB calculations near the measured E_F (E_F^m) and E_F^{off}. At larger E_B, the $E_B(\mathbf{k}_x)$ dispersion of U is close to that of band 2 in the calculations. Between $\overline{X}_2 - \overline{M}$ the $E_B(\mathbf{k}_x)$ dispersion of U would be expected to follow that of band 5 instead of band 2. However, feature U has the same $E_B(\mathbf{k}_x)$ dispersion between $\overline{\Gamma} - \overline{X}_1$ and $\overline{X}_2 - \overline{M}$, which is steeper than the $E_B(\mathbf{k}_x)$ dispersion of band 5. The origin of this discrepancy between the measured and calculated bands between $\overline{X}_2 - \overline{M}$ is not known. However, from the one-dimensionality of the surface states seen in figure 2(h), one can expect the $E_B(\mathbf{k}_x)$ dispersion of the features to be similar at different $\mathbf{k}_y$.

Feature A has been assigned to band 1 and the dark feature formed by more surface localised bulk states (dark blue solid arrows) in figure 2(b). In the calculations, band 1 overlaps with bulk states near E_F^{off}, but exists in the bulk band gap at larger E_B. In the measurements between $\overline{\Gamma} - \overline{X}_1$ feature A is in the bulk band gap near E_F^m, but overlaps with bulk states at larger E_B. This means that both band 1 and feature A can be thought of as surface states because parts of them exist in the bulk band gap. However, if a band has to be in the bulk band gap where it crosses the E_F to be counted as a E_F crossing, the calculated band 1 is not counted, but the measured feature A is counted between $\overline{\Gamma} - \overline{X}_1$. Between $\overline{X}_2 - \overline{M}$, feature A and the dark feature (dark blue solid arrows) in figure 2(b) exist in a region with bulk states. Thus, none of them are considered surface states contributing to the number of E_F crossings.

From the measurements at different photoexcitation energies, feature C appears to exist in the bulk bandgap between $\overline{\Gamma} - \overline{X}_1$ [50]. It follows two different, but closely spaced, $E_B(\mathbf{k}_x)$ dispersions (see details in the SM [50]). Furthermore, the gradient of its $E_B(\mathbf{k}_x)$ dispersion in figure 2(i) changes between being positive and negative, suggesting that the dispersion is vertical in some places. A vertical dispersion is unphysical for a single band since it would correspond to an electron with infinite Fermi velocity [61]. Thus, the shape of C suggests that at least two bands exist in the larger pink shaded region, but that these are very close together and therefore challenging to resolve [50]. The $\mathbf{k}_F^m$ of feature C agrees within uncertainties with the $\mathbf{k}_F^c$ of bands 2 and 3. This, together with its shape, suggests that feature C corresponds to bands 2 and 3. In the measurements, feature C is thought to sometimes indicate one of the bands and other times a point between the two bands. Presuming that feature C corresponds to bands 2 and 3, it is considered to contribute with two surface state E_F^m crossings between $\overline{\Gamma} - \overline{X}_1$.

Between $\overline{X}_2 - \overline{M}$, feature C is found to be in a region with bulk bands, but its surface character varies (see the SM [50]). This apparent mixture of more or less surface localised states agrees with the variation of the surface localisation along a given band in the calculated band structure, especially where the bands are close to each other or the bulk continuum. Since feature C is bulk-like near E_F^m, it is not considered a E_F^m crossing.

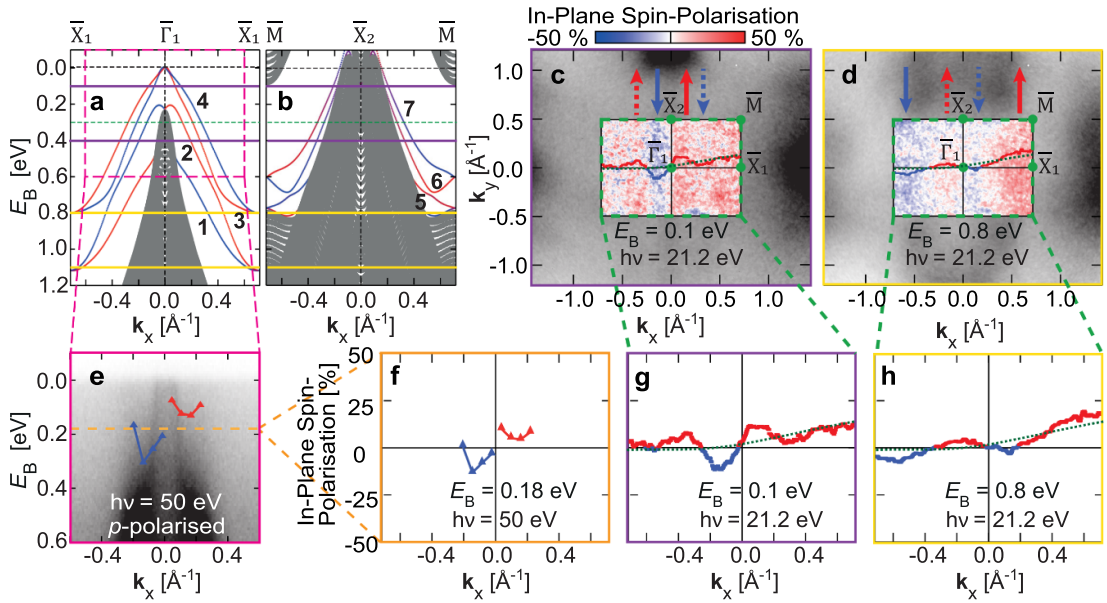

Figure 3. In-plane spin-polarisation of Sb(112) along $\pm\mathbf{k}_y$ ($\mathbf{S}_y$). In all panels red corresponds to spin along $+\mathbf{k}_y$ and blue to spin along $-\mathbf{k}_y$. (a) and (b) TB calculated spin-polarisation. The purple and yellow solid lines in (a) and (b) show where $E_B = 0.1$ eV and $E_B = 0.8$ eV are, respectively, relative to E_F^c (black dashed line) and E_F^{off} (green dashed line, see details in the text). (c) and (d) Spin-filtered constant energy surfaces (ESs) measured using a momentum microscope. Spin-averaged and spin-polarised ESs are shown outside and inside the 1st BZ, respectively. Red/blue arrows show the direction of the measured in-plane component of the spin-vector. (g) and (h) show the average spin-polarisation from MDCs at constant $\mathbf{k}_y$ inside the 1st BZ in (c) and (d), respectively. (c) and (g) were measured at $E_B = 0.1$ eV and (d) and (h) at $E_B = 0.8$ eV (see purple and yellow solid lines in (a)). Green dotted lines in (c), (d), (g) and (h) are guides to the eye showing where the zero-line of the spin-polarisation is expected to be (see details in the text). (e) Measured band structure inside the dashed pink rectangle in (a). The spin-polarisation at $E_B = 0.18$ eV has been overlaid and is given in (f).

Summarising, the measurements indicate in total four E_F^m crossings between $\overline{\Gamma} - \overline{X}_1$ (one from A, two from C and one from U) and one E_F^m crossing between $\overline{X}_2 - \overline{M}$ (from U), if only surface state crossings in the bulk bandgap are counted. Even if there are only two contour (or E_F^c) crossings between $\overline{\Gamma} - \overline{X}_1$ in the calculations, there is an even number of E_F crossings in both the measurements and calculations, in agreement with the predictions from topology. There are four bands crossing E_F^{off} in the calculations if the measurements are used to determine the surface character of the bands and where the E_F should be. Between $\overline{X}_2 - \overline{M}$ the measurements and calculations agree that there is only one crossing, regardless of whether E_F or contour crossings are considered. Hence, also between $\overline{X}_2 - \overline{M}$ the results are in agreement with conventional topological arguments. Still, without the calculations, it would have been challenging to deduce the number of bands assigned to C. Measurements at different photoexcitation energies were required to separate surface and bulk features. Even if both counting E_F crossings and contour crossings seem to suggest the same topology and agree with predictions from parity considerations, careful analysis and supporting theoretical predictions are ultimately required to yield definite answers.

The feature Y is only visible along the $\overline{X}_2 - \overline{M}$ direction in figures 2(j) and (l). Its E_B vs. $\mathbf{k}_x$ dispersion resembles band 7 in the calculations when following a path from $\overline{X}_2$ to $\overline{M}$, and appears to continue as band 6 between $\overline{M}$ and $\overline{X}_2$ in the neighbouring BZ (N. BZ). The measured E_B vs. $\mathbf{k}_x$ dispersion cross $\overline{M}$ at a larger E_B than that suggested in the calculations, again indicating that the measured features along $\overline{X}_2 - \overline{M}$ have a steeper $E_B(\mathbf{k}_x)$ dispersion than the calculated bands 5–7. In figure 2(d) bands 6 and 7 make an $\times$ centred at $\overline{M}$, but in the measurements only one of the legs in the $\times$ is visible. This is not surprising as the photoemission intensity is determined by the dipole matrix elements of the photoexcitation process, and may thus vary with photoexcitation energy, light polarisation and the geometry of the experiment [58]. Matrix element effects can therefore also breed difficulties in determining the number of E_F^m crossings. Intensity variations with $\mathbf{k}$ similar to that of feature Y, have been seen previously for spin-polarised bands, and may suggest that feature Y is spin-polarised [62, 63].

3.3. Spin-polarisation

Spin-polarisation is one of the characteristic properties of topological surface states [4]. The calculated and measured spin-polarisation of the surface states on Sb(112) have been summarised in figure 3. From the TB calculations, it was found that $\mathbf{S}_y$ pointing in-plane and along $\overline{\Gamma} - \overline{X}_2$, herein defined as $\pm\mathbf{k}_y$, is the strongest

spin-vector component. A positive (red) spin-polarisation in figure 3 means that the spin-vector points along $+\mathbf{k}_y$, and a negative (blue) spin-polarisation along $-\mathbf{k}_y$ as indicated by the arrows in figures 3(c) and (d).

Bands 2, 3, 5 and 6 have a positive spin-polarisation for positive values of $\mathbf{k}_x$ (along $\overline{\Gamma}-\overline{\mathrm{X}}_1$ and $\overline{\mathrm{X}}_2-\overline{\mathrm{M}}$) in figures 3(a) and (b), while bands 1, 4 and 7 have a negative spin-polarisation. At $-\mathbf{k}_x$ the spin-polarisation of the bands reverse.

The spin-polarisation was measured by acquiring spin-filtered constant ESs with a momentum microscope (figures 3(c), (d), (g) and (h)) [52], or by measuring the intensity from different spin-components along momentum distribution curves using two V-LEED detectors (figures 3(e) and (f)) [53]. The spin-measurements have a large uncertainty due to the weak intensity of the spin-polarised bands and variations in the detector efficiency. The weak intensity is most likely a consequence of Sb being semi-metallic. In materials with a bulk band gap, elastic scattering from bulk bands is negligible, the background is low, and it is possible to clearly resolve even weak states [64]. For Sb(112), the bulk states contribute to a high background. Since the intensity of the spin-polarised bands is weak compared to the background, quantitative estimates of the spin-polarisation are less accurate. Still, the spin-reversal can be used to qualitatively identify spin-polarised bands. The efficiency of the spin detector varies non-linearly across the detector, giving rise to an apparent increase in the spin-polarisation for positive $\mathbf{k}_x$ [50] and a larger uncertainty in the zero-line for the spin-polarisation. The green dotted line is added as a guide to the eye to show approximately where the zero-line is expected to be if the spin-reversal is assumed to be symmetric around $\mathbf{k}_x = 0\,\text{Å}^{-1}$. Additional information about the spin measurements and how the spin-polarisation was determined can be found in section 2 and the SM [50]. The measured spin-polarisation agrees with the calculations. In figures 3(c) and (d) the 1st BZs have been filled with the in-plane spin-polarisation measured at $E_\mathrm{B} = 0.1\,\text{eV}$ and $E_\mathrm{B} = 0.8\,\text{eV}$, respectively, as indicated by the purple and yellow solid lines in figures 3(a) and (b). There are two lines for each energy in figures 3(a) and (b), one relative to E_F^c (black dashed line, corresponding to the originally calculated electron occupancy), and one relative to $E_\mathrm{F}^\mathrm{off}$ (green dashed line, corresponding to an offset E_F matching better with the measurements). The images surrounding the 1st BZ in figures 3(c) and (d) show the spin-averaged intensity at the different energies as ESs [50]. The red/blue arrows in figures 3(c) and (d) mark spin-polarised states. The spin-polarisation along MDCs at each $\mathbf{k}_y$ in the 1st BZ in figures 3(c) and (d) were averaged and plotted in figures 3(g) and (h).

The spin-polarised states illustrated by solid arrows in figures 3(c) and (d) are close to $\mathbf{k}_x = 0\,\text{Å}^{-1}$ in figures 3(c) and (g), and closer to the BZ boundaries at $\mathbf{k}_x = \pm 0.715\,\text{Å}^{-1}$ in figures 3(d) and (h). The spin-polarisation of these states is approximately $\pm 11\,\%$. Since the spin-polarisation is positive (negative) for $+\mathbf{k}_x$ ($-\mathbf{k}_x$), it is similar to that of bands 2, 3, 5 and 6 in the calculations. Bands 2 and 3 are closer to $\overline{\Gamma}$ than band 4 between the two purple solid lines in figures 3(a) and (b), but closer to the BZ boundary than band 1 between the yellow solid lines. Hence, the spin-polarised calculated bands 2 and 3 are found at ($\mathbf{k}_x$, E_B) matching those of the spin-polarised measured features indicated by solid red/blue arrows. The spin-polarisation appears to be similar along $\overline{\Gamma}-\overline{\mathrm{X}}_1$ and $\overline{\mathrm{X}}_2-\overline{\mathrm{M}}$. Thus, the measurements suggest that there are spin-polarised bands at larger E_B also between $\overline{\mathrm{X}}_2-\overline{\mathrm{M}}$, even if there are no spin-polarised bands at $E_\mathrm{B} > 0.8\,\text{eV}$ in the TB calculations in figure 3(b). This is in agreement with the previous observation that the $E_\mathrm{B}(\mathbf{k}_x)$ dispersion of the measured features is steeper than expected from the calculations between $\overline{\mathrm{X}}_2-\overline{\mathrm{M}}$.

Band 1 does not show spin-polarisation between $E_\mathrm{B} \approx 0.1\,\text{eV}$ and $E_\mathrm{B} \approx 0.5\,\text{eV}$ in the TB model since it overlaps with bulk bands. However, when measuring the spin-polarisation of feature A, it is found to be spin-polarised with a spin-reversal of approximately $\pm 8\,\%$ as shown in figures 3(e) and (f). Thus, the spin-polarisation corroborates that band 1 is surface-like near E_F^c and $E_\mathrm{F}^\mathrm{off}$. Feature A is the only visible feature in figure 3(e) and its spin-reversal is almost identical to that near $\mathbf{k}_x = 0\,\text{Å}^{-1}$ in figure 3(g). Hence, if band 1 corresponds to feature A its spin-polarisation is similar to that of bands 2 and 3 for $E_\mathrm{B} \approx 0.2 - 0.5\,\text{eV}$ in figure 3(a), indicating that the spin-polarisation seen in figures 3(c) and (g) may also feature some signal from band 1.

The dashed red/blue arrows at $E_\mathrm{B} = 0.8\,\text{eV}$ in figure 3(d) indicate spin-polarised bands near $\mathbf{k}_x = \pm 0.1\,\text{Å}^{-1}$. The bands have a negative (positive) spin-polarisation for $+\mathbf{k}_x$ ($-\mathbf{k}_x$) and are closer to $\mathbf{k}_x = 0\,\text{Å}^{-1}$ than spin-polarised bands indicated by solid arrows (assigned to bands 2 and 3). Hence, the spin-polarised bands indicated by dashed arrows are similar to band 1 in the calculations. Their spin-polarisation is weak (around $\pm 2\,\%$, see figure 3(h)) maybe because they overlap with bulk bands or have an overall weaker intensity than neighbouring bands. Still, the spin-reversal is clear.

The bands illustrated by dashed red/blue arrows at $E_\mathrm{B} = 0.1\,\text{eV}$ in figure 3(c) also have a negative (positive) spin-polarisation for $+\mathbf{k}_x$ ($-\mathbf{k}_x$). However, they are found at $\mathbf{k}_x \approx \pm 0.3\,\text{Å}^{-1}$, and are therefore further from $\mathbf{k}_x = 0\,\text{Å}^{-1}$ than the spin-polarised bands indicated by solid arrows (assigned to bands 2 and 3). Thus, spin-polarised bands indicated by dashed arrows in figure 3(c) are reminiscent of bands 4 and 7 in the calculations. The averaged spin-polarisation in figure 3(g) is approximately $7\,\%$ at $\mathbf{k}_x \approx -0.3\,\text{Å}^{-1}$. Near $\mathbf{k}_x \approx +0.3\,\text{Å}^{-1}$, the averaged spin-polarisation is small ($\approx 3\,\%$), but not negative as one would expect for a

spin-reversal. Still, the spin-polarisation reduces as if it is reversing, and would presumably go below zero if we assumed the zero-line indicated by the green dotted line in figures 3(c), (d), (g) and (h).

Overall, the measured spin-polarisation can be correlated to the calculated spin-polarisation and the measured bands. It appears that features A, C and U, which were all found to be surface-like between $\overline{\Gamma} - \overline{X}_1$ in the measurements, are spin-polarised as one would expect for topological surface states.

4. Conclusion

ARPES measurements and TB calculations have shown that Sb(112) has at least two pairs of 1D, spin-polarised states reminiscent of those on vicinal Bi surfaces, TIs, TSMs and HOTIs. The shape and spin-polarisation of the measured features and the calculated bands agree, even if the measured features had a steeper energy dispersion and different $\mathbf{k}_F$ compared to the calculated bands. It was challenging to determine the number of E_F or contour crossings because the bands did not always have a pure surface or bulk character, and some of the bands were difficult to distinguish. The calculations and measurements still suggest that an even and odd number of surface states cross the measured E_F along $\overline{\Gamma} - \overline{X}_1$ and $\overline{X}_2 - \overline{M}$, respectively. Hence, Sb(112) appears to have topologically non-trivial surface states along $\overline{X}_2 - \overline{M}$.

This study highlights why ARPES has to be combined with theoretical efforts when it is used to evaluate the topology of vicinal semi-metals and other topological systems. The fact that bands may have a mix of surface and bulk character, or can be close together and thus hard to resolve, or that photoionisation matrix elements may strongly vary, all influence how easily the number of E_F or contour crossings can be counted. Despite this, we have shown how a careful and holistic approach can give a good understanding of the band structure and the topological nature of electronic states on surfaces of semi-metals.

Understanding these properties can be important when developing new technologies based on the properties of topological materials [4, 6–14]. Materials with robust one-dimensional and spin-polarised surface states have attracted particular attention because of their potential application in spintronics [4, 6, 12]. Sb(112) would be a good candidate for use in spintronic devices if the bulk bands could be shifted away from the E_F such that electronic transport would only be possible through its surface states. Future work could include efforts to modify Sb(112) to achieve this, or alternatively to investigate whether vicinal surfaces of TIs like $Bi_{1-x}Sb_x$ host similar states.

Data availability statement

The data cannot be made publicly available upon publication because they are not available in a format that is sufficiently accessible or reusable by other researchers. The data that support the findings of this study are available upon reasonable request from the authors.

Acknowledgments

This work was partly supported by the Research Council of Norway, Project Numbers 262633, 324183, 315330, and 335022. This research used ESM of the National Synchrotron Light Source II, a U S Department of Energy (DOE) Office of Science User Facility operated for the DOE Office of Science by Brookhaven National Laboratory under Contract No. DE-SC0012704. We acknowledge Elettra Sincrotrone Trieste for providing access to its synchrotron radiation facilities and for financial support under the IUS internal Project. We thank Ivana Vobornik and Jun Fujii for assistance in using beamline APE-LE at Elettra Sincrotrone Trieste.

ORCID iDs

A C Åsland 0000-0003-2837-6133
H I Røst 0000-0002-1853-8349
J Hu 0000-0002-2232-8440
J W Wells 0000-0001-6366-366X

References

[1] Blum V *et al* 2024 Roadmap on methods and software for electronic structure based simulations in chemistry and materials *Electron. Struct.* **6** 042501
[2] Burkov A A 2016 Topological semimetals *Nat. Mater.* **15** 1145–8
[3] Rachel S 2018 Interacting topological insulators: a review *Rep. Prog. Phys.* **81** 116501
[4] He M, Sun H and He Q L 2019 Topological insulator: spintronics and quantum computations *Front. Phys.* **14** 43401

[5] Lv B Q, Qian T and Ding H 2021 Experimental perspective on three-dimensional topological semimetals *Rev. Mod. Phys.* **93** 025002
[6] Hirohata A, Yamada K, Nakatani Y, Prejbeanu I-L, Diény B, Pirro P and Hillebrands B 2020 Review on spintronics: principles and device applications *J. Magn. Magn. Mater.* **509** 166711
[7] Fan T, Khang N H D, Nakano S and Hai P N 2022 Ultrahigh efficient spin orbit torque magnetization switching in fully sputtered topological insulator and ferromagnet multilayers *Sci. Rep.* **12** 2998
[8] Binda F, Fedel S, Alvarado S F, Noël P and Gambardella P 2023 Spin-orbit torques and spin Hall magnetoresistance generated by twin-free and amorphous $Bi_{0.9}Sb_{0.1}$ topological insulator films *Adv. Mater.* **35** 2304905
[9] Yun J and Xi Li 2024 Highly efficient spin current transport properties in spintronic devices based on topological insulator *Adv. Quantum Technol.* **7** 2400041
[10] Toriyama M Y and Snyder G J 2025 Topological insulators for thermoelectrics: a perspective from beneath the surface *Innovation* **6** 100782
[11] Krishnamoorthy H N S, Dubrovkin A M, Adamo G and Soci C 2023 Topological insulator metamaterials *Chem. Rev.* **123** 4416–42
[12] Guo Z, Wang Y, Shaolin K, Xiaoqiang S, Ren J and Chen H 2024 1D photonic topological insulators composed of split ring resonators a mini review *Adv. Phys. Res.* **3** 2300125
[13] Tairan Xi *et al* 2025 Terahertz sensing based on the nonlinear electrodynamics of the two-dimensional correlated topological semimetal $TaIrTe_4$ *Nat. Electron.* **8** 578–86
[14] Yu H, Zeng H, Zhang Y, Liu Y, ShangGuan W, Zhang X, Zhang Z and Zhang Y 2025 Two-dimensional layered topological semimetals for advanced electronics and optoelectronics *Adv. Funct. Mater.* **35** 2412913
[15] Murakami S 2006 Quantum spin Hall effect and enhanced magnetic response by spin-orbit coupling *Phys. Rev. Lett.* **97** 236805
[16] Hasan M Z and Kane C L 2010 Colloquium: topological insulators *Rev. Mod. Phys.* **82** 3045–67
[17] Qi X-L and Zhang S-C 2011 Topological insulators and superconductors *Rev. Mod. Phys.* **83** 1057–110
[18] Liu Y and Allen R E 1995 Electronic structure of the semimetals Bi and Sb *Phys. Rev. B* **52** 1566–77
[19] Fu L and Kane C L 2007 Topological insulators with inversion symmetry *Phys. Rev. B* **76** 045302
[20] Teo J C Y, Fu L and Kane C L 2008 Surface states and topological invariants in three-dimensional topological insulators: application to $Bi_{1-x}Sb_x$ *Phys. Rev. B* **78** 045426
[21] Wong M-H, Bian G, Miller T and Chiang T-C 2015 Topological phase transitions in antimony without gap parity reversal *Europhys. Lett.* **109** 17005
[22] Guo H *et al* 2011 Evolution of surface states in $Bi_{1-x}Sb_x$ alloys across the topological phase transition *Phys. Rev. B* **83** 201104
[23] Nouri N, Bieniek M, Brzezińska M, Modarresi M, Borujeni S Z, Rashedi G, Wójs A and Potasz P 2018 Topological phases in Bi/Sb planar and buckled honeycomb monolayers *Phys. Lett. A* **382** 2952–8
[24] Song Y-L, Shang S-X, Chen X-L, Zhang C-W and Zhang S-F 2024 Disorder-induced phase transitions in a two-dimensional magnetic topological insulator system *J. Phys.: Condens. Matter* **37** 095703
[25] Hsieh D, Qian D, Wray L, Xia Y, Hor Y S, Cava R J and Hasan M Z 2008 A topological dirac insulator in a quantum spin Hall phase *Nature* **452** 970–4
[26] Chuang F-C, Hsu C-H, Chen C-Y, Huang Z-Q, Ozolins V, Lin H and Bansil A 2013 Tunable topological electronic structures in Sb(111) bilayers: a first-principles study *Appl. Phys. Lett.* **102** 022424
[27] Jin K-H and Jhi S-H 2015 Quantum anomalous Hall and quantum spin-Hall phases in flattened Bi and Sb bilayers *Sci. Rep.* **5** 8426
[28] Kim S H, Jin K-H, Park J, Kim J S, Jhi S-H and Yeom H W 2016 Topological phase transition and quantum spin Hall edge states of antimony few layers *Sci. Rep.* **6** 33193
[29] Zhu S-Y *et al* 2019 Evidence of topological edge states in buckled antimonene monolayers *Nano Lett.* **19** 6323–9
[30] Radha S K and Lambrecht W R L 2020 Buckled honeycomb antimony: higher order topological insulator and its relation to the Kekulé lattice *Phys. Rev. B* **102** 115104
[31] Kukreti S, Ramawat S, Singh N and Dixit A 2023 Strain-engineered thermophysical properties ranging from band-insulating to topological insulating phases in β-antimonene *Nanoscale* **15** 13997–4006
[32] Sugawara K, Sato T, Souma S, Takahashi T, Arai M and Sasaki T 2006 Fermi surface and anisotropic spin-orbit coupling of Sb(111) studied by angle-resolved photoemission spectroscopy *Phys. Rev. Lett.* **96** 046411
[33] Hsieh D *et al* 2009 Observation of unconventional quantum spin textures in topological insulators *Science* **323** 919–22
[34] Bianchi M, Guan D, Stróżecka A, Voetmann C H, Bao S, Pascual J I, Eiguren A and Hofmann P 2012 Surface states on a topologically nontrivial semimetal: the case of Sb(110) *Phys. Rev. B* **85** 155431
[35] Stróżecka A, Eiguren A, Bianchi M, Guan D, Voetmann C H, Bao S, Hofmann P and Pascual J I 2012 Unconventional spin texture of a topologically nontrivial semimetal Sb(110) *New J. Phys.* **14** 103026
[36] Kane C L and Mele E J 2005 Z_2 topological order and the quantum spin Hall effect *Phys. Rev. Lett.* **95** 146802
[37] König M, Wiedmann S, Brüne C, Roth A, Buhmann H, Molenkamp L W, Qi X-L and Zhang S-C 2007 Quantum spin Hall insulator state in HgTe quantum wells *Science* **318** 766–70
[38] Wells J W *et al* 2009 Nondegenerate metallic states on Bi(114): a one-dimensional topological metal *Phys. Rev. Lett.* **102** 096802
[39] Burkov A A, Hook M D and Balents L 2011 Topological nodal semimetals *Phys. Rev. B* **84** 235126
[40] Leuenberger D, Yanagisawa H, Roth S, Dil J H, Wells J W, Hofmann P, Osterwalder J and Hengsberger M 2013 Excitation of coherent phonons in the one-dimensional Bi(114) surface *Phys. Rev. Lett.* **110** 136806
[41] Bianchi M *et al* 2015 One-dimensional spin texture of Bi(441): quantum spin Hall properties without a topological insulator *Phys. Rev. B* **91** 165307
[42] Neupane M *et al* 2016 Observation of topological nodal fermion semimetal phase in ZrSiS *Phys. Rev. B* **93** 201104
[43] Schindler F, Cook A M, Vergniory M G, Wang Z, Parkin S S P, Bernevig B A and Neupert T 2018 Higher-order topological insulators *Sci. Adv.* **4** eaat0346
[44] Schindler F *et al* 2018-09 Higher-order topology in bismuth *Nat. Phys.* **14** 918–24
[45] Shao Y *et al* 2019 Optical signatures of Dirac nodal lines in $NbAs_2$ *Proc. Natl Acad. Sci. USA* **116** 1168–73
[46] Åsland A C *et al* 2023 One-dimensional spin-polarized surface states: a comparison of Bi(112) with other vicinal bismuth surfaces *Phys. Rev. B* **108** 205403
[47] Lee J, Kwon J, Lee E, Park J, Cha S, Watanabe K, Taniguchi T, Jo M-H and Choi H 2023 Spinful hinge states in the higher-order topological insulators WTe_2 *Nat. Commun.* **14** 1801
[48] Yang Y-B, Wang J-H, Li K and Xu Y 2024 Higher-order topological phases in crystalline and non-crystalline systems: a review *J. Phys.: Condens. Matter* **36** 283002
[49] Mao Y-F, Tao Y-L, Wang J-H, Zeng Q-B and Xu Y 2024 Higher-order topological insulators in three dimensions without crystalline counterparts *Phys. Rev. B* **109** 134205

[50] See the supplementary material at https://iopscience.iop.org/article/10.1088/2516-1075/adf384 which includes [18, 46, 51–53, 65–69] for details about the spin-filtered measurements and analysis, TB calculations, LEED measurements, how the E_F^m and E_F^{eff} was determined, and how measurements at different photoexcitation energies were used to investigate the surface character of the bands.
[51] Kirschner J, Giebels F, Gollisch H and Feder R 2013 Spin-polarized electron scattering from pseudomorphic Au on Ir(001) *Phys. Rev. B* **88** 125419
[52] Tusche C, Krasyuk A and Kirschner J 2015 Spin resolved bandstructure imaging with a high resolution momentum microscope *Ultramicroscopy* **159** 520–9
[53] Bigi C *et al* 2017 Very efficient spin polarization analysis (VESPA): new exchange scattering-based setup for spin-resolved ARPES at APE-NFFA beamline at Elettra *J. Synchrotron Radiat.* **24** 750–6
[54] Zhu X-G and Hofmann P 2014 Topological surface states on $Bi_{1-x}Sb_x$: dependence on surface orientation, termination and stability *Phys. Rev. B* **89** 125402
[55] Kevan S D and Eberhardt W 1992 *Angle-Resolved Photoemission: Theory and Current Applications* (Elsevier Amsterdam)
[56] Hofmann P 2016 *Surface Physics: An Introduction* (Philip Hofmann)
[57] Himpsel F J 1980 Experimental determination of bulk energy band dispersions *Appl. Opt.* **19** 3964–70
[58] Damascelli A 2004 Probing the electronic structure of complex systems by ARPES *Phys. Scr.* **2004** 61
[59] Mazzola F, Polley C M, Miwa J A, Simmons M Y and Wells J W 2014 Disentangling phonon and impurity interactions in δ-doped Si(001) *Appl. Phys. Lett.* **104** 173108
[60] Papaconstantopoulos D A and Mehl M J 2003 The Slater-Koster tight-binding method: a computationally efficient and accurate approach *J. Phys.: Condens. Matter* **15** R413
[61] Kittel C and McEuen P 2018 *Introduction to Solid State Physics* (Wiley)
[62] Gierz I, Henk J, Höchst H, Ast C R and Kern K 2011 Illuminating the dark corridor in graphene: polarization dependence of angle-resolved photoemission spectroscopy on graphene *Phys. Rev. B* **83** 121408
[63] Yaji K, Kuroda K, Toyohisa S, Harasawa A, Ishida Y, Watanabe S, Chen C, Kobayashi K, Komori F and Shin S 2017 Spin-dependent quantum interference in photoemission process from spin-orbit coupled states *Nat. Commun.* **8** 14588
[64] Miwa J A, Warschkow O, Carter D J, Marks N A, Mazzola F, Simmons M Y and Wells J W 2014 Valley splitting in a silicon quantum device platform *Nano Lett.* **14** 1515–9
[65] Sherman N 1956 Coulomb scattering of relativistic electrons by point nuclei *Phys. Rev.* **103** 1601–7
[66] Meier F, Dil J H and Osterwalder J 2009 Measuring spin polarization vectors in angle-resolved photoemission spectroscopy *New J. Phys.* **11** 125008
[67] Crystal Maker Software Ltd 2023 Single crystal 4 (available at: https://crystalmaker.com//singlecrystal/I)
[68] Hofmann P *et al* 2019 Strong-coupling charge density wave in a one-dimensional topological metal *Phys. Rev. B* **99** 035438
[69] Kim T K *et al* 2005 Evidence against a charge density wave on Bi(111) *Phys. Rev. B* **72** 085440